


RESEARCH PAPER

An essential role for mannan degradation in both cell growth and secondary cell wall formation

Rui Zhang^{1,2,†}, Bo Li^{1,2,†}, Yunjun Zhao¹, Yingying Zhu^{3,*}, and Laigeng Li^{1,*} 

¹ National Key Laboratory of Plant Molecular Genetics, CAS Center for Excellence in Molecular Plant Sciences, Chinese Academy of Sciences, Shanghai 200032, China

² University of the Chinese Academy of Sciences, Beijing 100049, China

³ State Key Laboratory of Herbage Improvement and Grassland Agro-ecosystems and College of Ecology, Lanzhou University, Lanzhou 730000, Gansu, China

† These authors contributed equally to this work.

* Correspondence: zhuyy@lzu.edu.cn or lgli@cemps.ac.cn

Received 5 May 2023; Editorial decision 15 November 2023; Accepted 17 November 2023

Editor: Simon Turner, University of Manchester, UK

Abstract

Coordination of secondary cell wall deposition and cell expansion during plant growth is required for cell development, particularly in vascular tissues. Yet the fundamental coordination process has received little attention. We observed that the *Arabidopsis* endo-1,4-mannanase gene, *AtMAN6*, is involved in the formation of cell walls in vascular tissues. In the inflorescence stem, the *man6* mutant had smaller vessel cells with thicker secondary cell walls and shorter fiber cells. Elongation growth was reduced in the root, and secondary cell wall deposition in vessel cells occurred early. Overexpression of *AtMAN6* resulted in the inverse phenotypes of the *man6* mutant. *AtMAN6* was discovered on the plasma membrane and was specifically expressed in vessel cells during its early development. The *AtMAN6* protein degraded galactoglucomannan to produce oligosaccharides, which caused secondary cell wall deposition in vessel and fiber cells to be suppressed. Transcriptome analysis revealed that the expression of genes involved in the regulation of secondary cell wall synthesis was changed in both *man6* mutant and *AtMAN6* overexpression plants. *AtMAN6*'s C-terminal cysteine repeat motif (CCRM) was found to facilitate homodimerization and is required for its activity. According to the findings, the oligosaccharides produced by *AtMAN6* hydrolysis may act as a signal to mediate this coordination between cell growth and secondary cell wall deposition.

Keywords: Cell expansion, endo- β -1,4-mannanase, oligosaccharides, secondary cell wall, xylem.

Introduction

Plant cell walls are carbohydrate-rich structures that surround plant cells and have a great constructional plasticity. Cell walls influence cell development and shape, intercellular communication, and the mechanical qualities of plant tissues and organs

(Barnes and Anderson, 2018; Wolf, 2022). Primary cell walls (PCWs) and secondary cell walls (SCWs) are the two types of plant cell walls. The PCW, which encases all plant cells, is flexible and extensible, allowing for cell expansion. SCWs, on

the other hand, are rigid and are deposited between the PCW and the plasma membrane in specialized cells such as vessel and fiber cells in vascular tissue to give mechanical strength and water-conducting ability (Meents *et al.*, 2018). In general, once the SCW is deposited, its stiffness stops the cell from changing form and size further. As a result, therefore, remodeling of the PCW and deposition of the SCW must be coordinated during plant growth and development.

Cell expansion is controlled by remodeling of the PCWs via secreted proteins that loosen and tighten the polysaccharide networks and links between various wall polymers such as cellulose, hemicelluloses, and pectin (Cosgrove, 2016, 2022). Several enzymes and wall-active proteins, such as expansins, family-9 and -12 endoglucanases, and family-16 xyloglucan endotransglucosylase/hydrolase (XTH), have been implicated in initial cell wall loosening and remodeling for cell expansion (Cosgrove, 2016). Some of these wall-loosening proteins, such as expansins and Cel12, work on 'biomechanical hotspots', which are limited cellulose-cellulose junctions held together by a xyloglucan-cellulose amalgam (Park and Cosgrove, 2012). Mannans and glucomannans, in addition to xyloglucan, which is the most common hemicellulose in the PCWs of spermatophytes except for grasses, are involved in the creation of the cell wall polysaccharide network by joining cellulose microfibrils (Whitney *et al.*, 1998; Yu *et al.*, 2018). Mannans have a linear backbone of β -1,4-linked mannose (Man) residues, whereas glucomannans have glucose (Glc) and Man residues (Moreira and Filho, 2008; Scheller and Ulvskov, 2010). The Man residues in the backbone of mannans and glucomannans can be substituted at O-6 with galactose (Gal), resulting in galactoglucomannan (GGM). GGM is found in moderate amounts in various angiosperm plant PCWs and in abundance in gymnosperm SCWs (Puls, 1997; Yu *et al.*, 2018). Recently, the molecule β -GGM has been observed to possess distinct structural features, including disaccharide side chains consisting of β -Gal- α -Gal and alternating Glc-Man repeats in the backbone. β -GGM has been found to have a role in cell expansion in conjunction with xyloglucan (Yu *et al.*, 2022).

SCWs are predominantly made up of cellulose, hemicellulose, and lignin (Meents *et al.*, 2018). SCW deposition is closely regulated by a complex network of transcription factors (TFs) and their target genes for the biosynthesis of distinct SCW components (Zhu and Li, 2021). This network is made up of three different 'layers' of TFs. The top layer consists of master TFs VASCULAR NAC DOMAIN (VND1-VND7), which regulate SCW biosynthesis in vessel cells, and the NAC SECONDARY WALL THICKENINGS (NST1 and NST3/SND1), which regulate SCW biosynthesis specifically in fiber cells (Kubo *et al.*, 2005; Mitsuda *et al.*, 2005; Zhong *et al.*, 2006, 2007; Yamaguchi *et al.*, 2008). These TFs control the secondary layer MYB TFs MYB46 and MYB83 (McCarthy *et al.*, 2009). Furthermore, those MYBs target a group of third-layer TFs that target specific cellulose biosynthesis genes, such as *CESA4*, *CESA7*, and *CESA8*, as well as lignin biosynthesis genes, such as

4CL and *PAL* genes (Rao and Dixon, 2018; Zhong *et al.*, 2019). After cells reach a particular size, SCW deposition begins. How do cells determine when to begin SCW biosynthesis? Signaling may be necessary in wall-thickened cells to coordinate cell expansion and SCW deposition. We discovered previously that *Populus* MAN6, an endo-mannanase, is localized on the plasma membrane with its active domain outside the plasma membrane and hydrolyzes the mannan linkage in the cell wall to produce oligosaccharides, which may function as a signal to regulate cell expansion and SCW formation during *Populus* xylem development (Zhao *et al.*, 2013a). Additionally, *Populus* MAN6 contains a conserved C-terminal region that is not found in other MAN genes and has an ortholog in Arabidopsis, although its genetic function is unknown (Zhao *et al.*, 2013b). In other investigations, galactoglucomannan oligosaccharides (GGMOs) enhanced the proportion of longitudinally divided cells developing into metaxylem cells in *Zinnia* xylogenesis suspension culture (Benová-Kákosová *et al.*, 2006). Exogenous GGMO treatment of mung bean seedlings causes cell elongation and delays xylem development in roots (Kollárová *et al.*, 2010). The genetic characterization of the MAN6-mediated regulation of cell expansion and SCW formation, however, is lacking.

In this study, we used genetic analysis to reveal that *AtMAN6*, which encodes an endo-1,4-mannanase in Arabidopsis, plays an important role in coordinating cell growth with SCW deposition during vascular development. We show that *AtMAN6* catalyzes the hydrolysis of mannan polysaccharides to enlarge vessel cells and create GGMOs, which may operate as extracellular signaling molecules to repress the SCW biosynthesis transcriptional network in both vessel and neighboring fiber cells during xylem development. This study revealed new information about the coordinated regulation of cell enlargement and SCW deposition during vascular development.

Materials and methods

Plant materials and growth conditions

The T-DNA insertion Arabidopsis line *man6* (SALK_129977) was obtained from the Salk Institute Genomic Analysis Laboratory (<http://signal.salk.edu>). The presence of the T-DNA insertion at the third exon in *man6* was confirmed by PCR and the expression level was determined by reverse transcription quantitative-PCR (RT-qPCR) (Supplementary Fig. S1A, B) using the primer sets listed in Supplementary Table S1. All Arabidopsis plants were in the Columbia-0 (Col-0) background. Arabidopsis seeds were sterilized for 15 min with 3% (v/v) sodium hypochlorite and then rinsed three times with sterile water. All seeds were plated on MS medium (4.4 g l⁻¹ Murashige and Skoog salt combination, 1% sucrose, and 0.8% agar, pH 5.7) and stratified at 4 °C for 2 d. Seedlings were grown on vertically positioned plates in a phytotron for 7 d at 22 °C under a light and dark cycle of 16/8 h, and then planted in soil and grown under the same conditions as described above.

Plasmid constructs generation and plant transformation

The coding sequence (1347 bp) or the promoter sequence (1500 bp) of the *AtMAN6* gene (*At5g01930*) was cloned into the *pMD19-T* vector (CB111; TransGen Biotech) using the primers listed in Supplementary

Table S1. The *AtMAN6* promoter sequence was cloned into the *pBI121* vector to replace the 35S promoter and generate *AtMAN6pro:GUS*. The *AtMAN6* coding region fused with the 7× MYC tag was reassembled into the *pCambia2300* vector to create constructs of *35S:AtMAN6-7×MYC*. For *35S:AtMAN6-GFP* generation, the *AtMAN6* coding sequence (CDS) was subcloned into the *pA7* vector, together with the cut 35S promoter, *AtMAN6* CDS, and green fluorescent protein (GFP), then assembled into the *pCambia2300* vector. The 35S promoter of *35S:AtMAN6-GFP* was replaced with the *AtMAN6* promoter to create *AtMAN6pro:AtMAN6-GFP*. The floral dip procedure (Clough and Bent, 1998) was used to transfer the constructs into wild-type (WT) plants.

The C-terminal truncated *AtMAN6* sequence was amplified by PCR (designated *AtMAN6-ΔC26*), which was then cloned into the *pCambia2300* vector to generate *35S:AtMAN6-ΔC26-GFP*. For mutation analysis, cysteines at the 12th and 222nd positions were replaced with serine to yield *AtMAN6-C12S*, and cysteines at the 423rd, 427th, and 431st positions in the conserved C-terminal cysteine repeat motif were replaced with serine to yield *AtMAN6-C345S*. The *35S:AtMAN6-C12S* and *35S:AtMAN6-C345S* constructs were created by reassembling the *AtMAN6-C12S* and *AtMAN6-C345S* cassettes into the *pCambia2300* vector. The *35S:GFP*, *35S:AtMAN6-GFP*, *35S:AtMAN6-Δ26-GFP*, *35S:AtMAN6-C12S-GFP*, and *35S:AtMAN6-C345S-GFP* were expressed in tobacco leaves (Sparkes et al., 2006) and used for subcellular localization observation using a laser confocal microscope (FV1000; Olympus) or protein extraction for enzymatic activity assessment.

RT-qPCR and β-glucuronidase staining

Roots, inflorescence stems, leaves, flowers, and siliques of 25-day-old WT plants were collected and ground into powder in liquid nitrogen using an automatic tissue grinder (Tissuelyser-48; JingXin). The E.Z.N.A Plant RNA Kit was used to isolate total RNA (R6827; Omega Bio-tek). TransScript One-Step gDNA Removal and cDNA Synthesis SuperMix (AT311; TransGen Biotech) was used to create cDNA from 100 ng of total RNA. For each gene, three biological replicates and three technical replicates were used. The specificity and amplification efficiency of gene-specific primers (Supplementary Table S1) were tested. RT-qPCR was performed on an iQ5 Real-Time PCR Detection System (Bio-Rad) using the UNICONTM qPCR SYBR Green Master Mix (Yeasen Biotech) and normalized to *AtActin2* (*At3g18780*). The $2^{-\Delta Ct}$ method was used to analyze gene expression.

Five independent T₃ lines of *AtMAN6pro:GUS* transgenic plants were collected for GUS staining. Hand-cut sections of roots, seedlings, rosette leaves, opened flowers, and inflorescence stems (5 cm above the base) of transgenic plants were incubated in 90% (v/v) acetone for 10 min and then rinsed three times with distilled water and incubated in GUS staining solution [100 mM sodium phosphate (pH 7), 10 mM EDTA, 0.5 mM ferricyanide, 0.5 mM ferrocyanide, 0.1% (v/v) Triton X-100, 20% (v/v) methanol, and 2 mM X-Gluc]. Sections were cleaned with 75% ethanol and then examined and photographed under a dissecting microscope (SZX7; Olympus).

Antibody production and immunolocalization

The C-terminal coding region of *AtMAN6* from amino acids 341 to 448 was subcloned into the *pET26b* vector for a polypeptide to be used as an antigen, which was produced, purified, and utilized in rabbits to raise polyclonal antibodies (YouKe Biotech). To examine the specificity of *AtMAN6* antibodies, inflorescence stems (*35S:AtMAN6*) and rosette leaves (*35S:AtMAN6-7×MYC*) of 3-week-old transgenic Arabidopsis plants as well as WT plants were collected and ground into a powder with liquid nitrogen and then mixed with an equal volume of 2× loading buffer [0.1 M Tris-HCl (pH 6.8), 4% SDS, 0.2% bromophenol blue, and 20% glycerol]. Proteins were electro-transferred onto a polyvinylidene

difluoride membrane and incubated with anti-*AtMAN6* (1:500 dilution) and anti-Actin (1:2000 dilution) monoclonal antibodies (M20009L; Abmart) and anti-MYC (1:2000 dilution) antibodies (T55537M; Abmart), as described in the established method (Song et al., 2010). Then, the polyvinylidene difluoride membranes were incubated in 10% NBT (nitro blue tetrazolium) and BCIP (5-bromo-4-chloro-3-indolyl phosphate) buffer to detect the protein band (Supplementary Fig. S2). Fresh segments (2 mm) of the inflorescence stems from WT plants were fixed in cold acetone for the immunolocalization experiment, embedded in paraffin and cut into 10 μm thick slides using a microtome (RM2235; Leica), as in Tang et al. (2006). The slides were dewaxed, rehydrated, and blocked, and incubated with anti-*AtMAN6* antibodies (1:500 dilution) or pre-immunized IgG as a negative control, followed by washing and incubation with NBT/BCIP buffer, and finally photographed (BX51; Olympus).

Cell wall analysis

Hand-cut cross sections of Arabidopsis inflorescence stems were stained for 3 min with 0.5% (w/v) phloroglucinol in 12% HCl, a lignin-specific dye, to visualize SCWs of vessel cells and fiber cells, and immediately examined under a bright-field microscope (BX51; Olympus). Arabidopsis inflorescence stems (1 cm from the base) from 4-week-old plants were cut into 2 mm pieces for ultrathin sectioning and TEM analysis (H-7650; Hitachi; Kyoto, Japan), as previously described (Song et al., 2010). ImageJ was used to quantify cell wall thickness using transmission electron micrographs (Zhao et al., 2013a). Inflorescence stem segments (1 cm from the base) of 4-week-old Arabidopsis plants were obtained for fiber cell morphological characterization as previously described (Yu et al., 2013, 2014). The inflorescence stems of 4-week-old Arabidopsis plants were tested for tensile breaking force (Yu et al., 2014). The inflorescence stem segments (10 cm from the base) of 5-week-old Arabidopsis plants were harvested for chemical examination of cell wall components such as ABSL (acetyl bromide-soluble lignin) content, crystalline cellulose content, and hemicellulose monosaccharide composition using previously described procedures (Foster et al., 2010a; b; Luo et al., 2021).

AtMAN6 enzymatic activity assay and GGMO proportion analysis

The WT and *35S:AtMAN6* transgenic Arabidopsis rosette leaves were used to extract total proteins, including the *AtMAN6* protein. The activity of *AtMAN6* was investigated using the substrates, and the proportion of GGMO products from GGM hydrolysis by *AtMAN6* protein was analyzed via HPLC/QTOF (quadruple time of flight)-MS and by endo-1,4-mannanase (E-BMANN) from *Aspergillus niger* as a control as described (Zhao et al., 2013a, b).

GGMO treatment assay

Crude GGM was isolated from *Populus* xylem and digested with plant-sourced *AtMAN6* proteins to produce GGMOs according to the description by Zhao et al. (2013a, b). WT Arabidopsis seeds were cultivated for 7 d on MS medium with 0.2 mg ml⁻¹ GGMOs-Man6 or GGMOs-EMan (1:100 dilution) and 1 mM NaAc as a control. The roots were then dyed with 0.1 g l⁻¹ propidium iodide (PI) for 30 s and examined and photographed using a laser confocal microscope (FV1000; Olympus). The 2 cm long bolting inflorescence stems of WT plants were detached from the base and incubated in 200 μl of 0.2 mg ml⁻¹ GGMOs-Man6 or GGMOs-EMan (in NaAc), or 1 mM NaAc as a control, and kept in a chamber with a 16/8 h light and dark cycle at 22 °C for 3 d. Finally, the treated inflorescence stems were cross-hand-cut, stained with phloroglucinol-HCl and observed for lignin deposition in SCWs of vessel and fiber cells.

RNA sequencing and gene expression profiling

The *man6* mutant, *35S:AtMAN6-7×MYC* Arabidopsis, and the WT were grown for 3 weeks. Pieces of the inflorescence stem from 10 cm above the base without leaves, flowers, and silique were collected for total RNA isolation using the E.Z.N.A Plant RNA Kit (R6827; Omega Bio-tek). All total RNA samples were treated with DNase I during extraction. RNA quality and concentration (>200 ng μl^{-1}) were examined by electrophoresis, and cDNA from 50 ng of total RNA was generated. Then 3 μg of the cDNA was fragmented, and 400 ng of the fragmented cDNA with an average size of 400 bp was used for library preparation (QiaQuick PCR extraction kit; QIAGEN). The libraries from each genotype were sequenced on an Illumina HiSeq 2000 (100 base paired-end reads). After filtering, the clean Illumina sequencing reads were mapped to the TAIR10 Arabidopsis genome using SOAPaligner/soap2. The RPKM (reads per kilobase per million reads) method was used to determine gene differential expression [fold change >2 ; false discovery rate (FDR) 0.001].

Identification of homologs of AtMAN6

The nucleic acid sequences of *AtMAN6* homologs in the presented species were identified in the JGI database (<http://www.phytozome.net>). ClustalW was used to examine their deduced protein sequences (<http://www.ebi.ac.uk/Tools/msa/clustalw2/>).

Results

AtMAN6 promotes cell expansion and delays deposition of SCW in vascular tissue

In order to examine the genetic function of *MAN6* in regulation of cell wall formation, the T-DNA insertion mutant *man6* (SALK_129977) and transgenic Arabidopsis (*MAN6* overexpression, OE-1 and OE-4, two separate lines with strong transgene expression) were collected and generated for characterization of their inflorescence stem growth (Supplementary Fig. S1A–D). The inflorescence stem in the 4-week-old *MAN6* overexpression plants bends downwards significantly, whereas that in the *man6* mutant is as straight as in the WT (Fig. 1A). A tensile breaking test was used to determine the strength of the inflorescence stem. The *man6* mutant had more strength than the WT, whereas OE plants had $\sim 33\%$ less strength than the WT (Fig. 1E). Cross-sections of the inflorescence stem at the base were examined, and lignin staining revealed that deposition of SCW in the vascular tissues was increased in the *man6* mutant compared with the WT (Fig. 1B). The lignin staining in vascular tissues was substantially less in OE plants than in the WT, particularly in xylem fiber cells near vessel cells and interfascicular fiber cells (Fig. 1B). The *man6* mutant had smaller vessel cells and shorter fibers than the WT, but the OE plants had larger vessel cells and longer fibers (Fig. 1F, G). The appearance of cell walls of vascular cells was examined using TEM (Fig. 1C, D). The thickness of SCWs in xylem vessels, xylem fibers, and interfascicular fiber cells was significantly increased in the *man6* mutant, whereas it was reduced by up to 50% in the OE plants (Fig. 1H). The analysis of the cell wall composition demonstrated that the *man6* mutant exhibited a notable increase in lignin and crystalline cellulose content, while the OE

plants displayed a decrease in comparison with the WT (Fig. 1I, J). The *man6* mutant exhibited a significantly higher concentration of Xyl and Man, which are the primary constituents of SCW xylan and mannan, respectively. In contrast, the OE plants displayed a reduced amount of Xyl and Man compared with the WT plants, as seen in Table 1. During root development, the primary root of 7-day-old *man6* mutant seedlings was 20% shorter than that of the WT, while the primary root of the OE plants was 20% longer than that of the WT (Fig. 2A, D). The root apical meristem of the *man6* mutant and OE plants stayed the same as that of the WT (Supplementary Fig. S1E). However, the number of cells in the elongation zone prior to vessel cell occurrence decreased by $>20\%$ in the *man6* mutant but increased by 25–27% in the OE plants when compared with the WT (Fig. 2B, E), indicating that SCW deposition in the vessel cells was advanced in the *man6* mutant but delayed in the OE plants. Furthermore, the length of the cortex cells in the maturation zone of the *man6* mutant was $\sim 20\%$ shorter than in the WT, whereas cells in the OE plants were 20% longer (Fig. 2C, F), demonstrating that *AtMAN6* plays a role in cell expansion. These findings suggested that *AtMAN6* could promote cell elongation while delaying SCW deposition in both inflorescence stem and root vascular tissues.

AtMAN6 was expressed particularly in growing vessel cells of vascular tissues

The transcriptional expression profiles of *AtMAN6* and the other six *MAN* genes were examined in the inflorescence stem, root, rosette leaf, flower, and silique. When compared with other analyzed tissues, *AtMAN6* has the highest expression level in the inflorescence stem (Fig. 3A; Supplementary Fig. S3), while *AtMAN1* was specifically expressed in the root, *AtMAN3* and *AtMAN7* in the flower, and *AtMAN2* and *AtMAN5* were ubiquitously expressed in the examined tissues. *AtMAN4* was scarcely expressed in the tissues studied (Supplementary Fig. S3). To investigate the expression specificity of *AtMAN6*, *AtMAN6pro::GUS* transgenic Arabidopsis lines were generated, and GUS staining revealed that GUS activity appeared particularly in the vascular tissues of the inflorescence stem, root, leaf vein, petals, and stamen (Fig. 3B–G). A comprehensive analysis of the inflorescence stem's vascular bundles revealed that GUS activity was only discovered in vessel cells near to cambium, and no GUS signal was detected in any other cells (Fig. 3B). Furthermore, the GUS staining signal appeared first in protoxylem vessel cells in the root stele, then faded and became evident only in metaxylem vessel cells when they appeared (Fig. 3C–E). Furthermore, an immunolocalization experiment using an *AtMAN6*-specific antibody (Supplementary Fig. S2) revealed that *AtMAN6* protein was only found in vessel cells of vascular tissues in inflorescence stem cells (Fig. 4A–C). GFP signals in *AtMAN6pro::AtMAN6-GFP* transgenic Arabidopsis revealed the spatial-specific localization of *AtMAN6* in root protoxylem and metaxylem vessels (Fig. 4D, E).

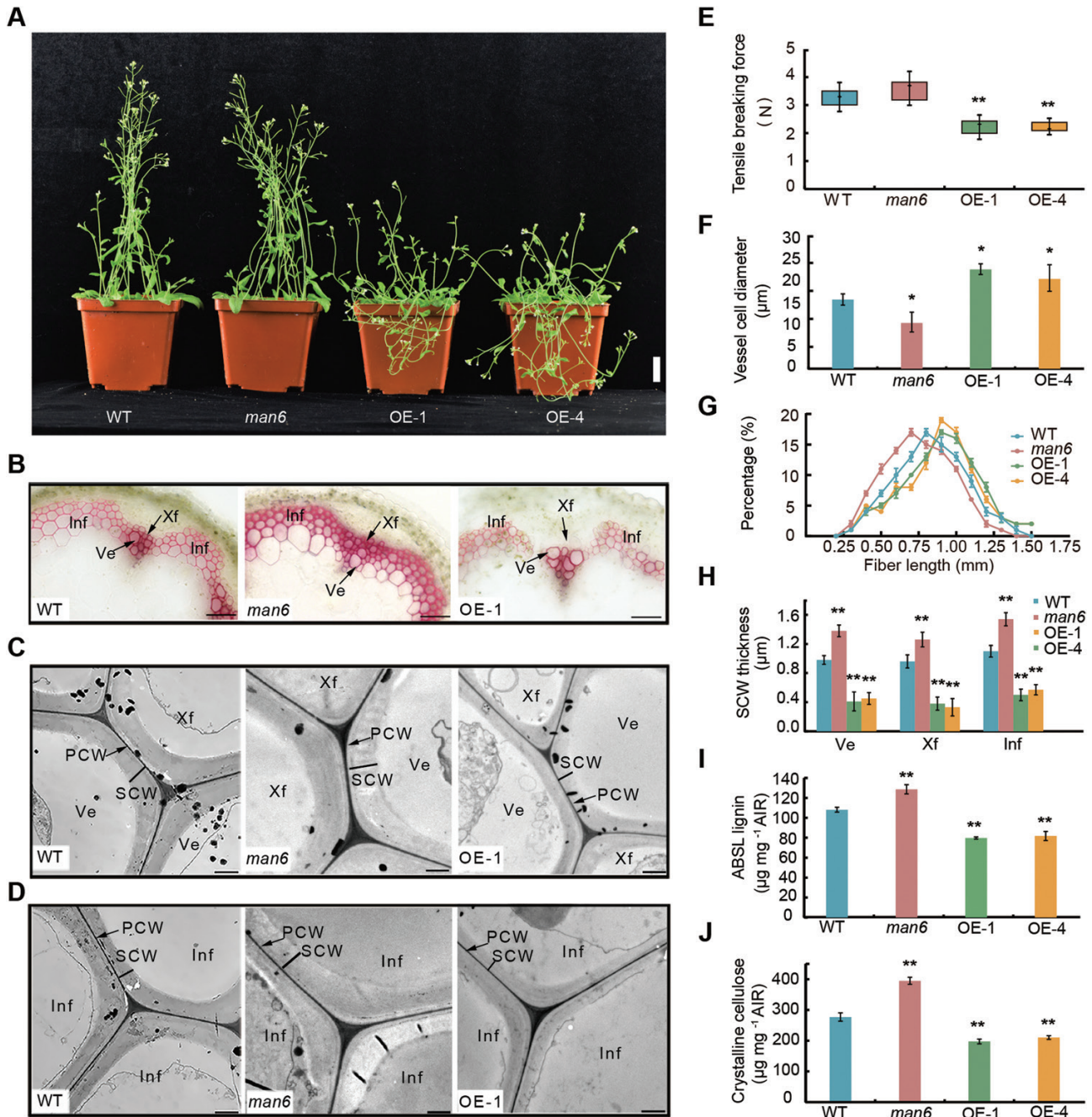


Fig. 1. The effect of *AtMAN6* on cell elongation and SCW deposition in inflorescence stem vascular cells. (A) Wild-type, *man6*, and *AtMAN6* overexpression (OE-1 and OE-4) plants at 4 weeks old. Bar=2 cm. (B) Lignin staining with 0.5% (w/v) phloroglucinol in 12% HCl on the inflorescence stem from the wild type, *man6*, and *AtMAN6* OE-1. Bar=50 μm. (C) SCWs of xylem vessel cells from the wild type, *man6*, and *AtMAN6* OE-1 imaged by TEM. Bar=1 μm. (D) SCWs of interfascicular fiber cells from the wild type, *man6*, and *AtMAN6* OE-1 imaged by TEM. Bar=1 μm. (E) Inflorescence stem tensile breaking test in wild-type, *man6*, and *AtMAN6* overexpression plants. The values represent means ±SE, *n*=30. (F) Inflorescence stem vessel cell diameter in wild-type, *man6*, and *AtMAN6* overexpression plants. The values represent means ±SE, *n*=30. (G) Inflorescence stem fiber cell length in wild-type, *man6*, and *AtMAN6* overexpression plants. The values represent means ±SE, *n*=300. (H) SCW thickness of vascular cells. The values represent means ±SE, *n*=30. (I) ABSL contents in wild-type, *man6*, and *AtMAN6* overexpression plants. The values represent means ±SE, *n*=3. Samples from 30 individual plants were combined for testing. (J) Crystalline cellulose contents in wild-type, *man6*, and *AtMAN6* overexpression plants. The values represent means ±SE, *n*=3. Samples from 30 individual plants were combined for testing. Ve, vessel cell; Xf, xylem fiber cell; Inf, interfascicular fiber cell; PCW, primary cell wall; SCW, secondary cell wall. Significance was determined by Fisher's LSD, **P*<0.05, ***P*<0.01.

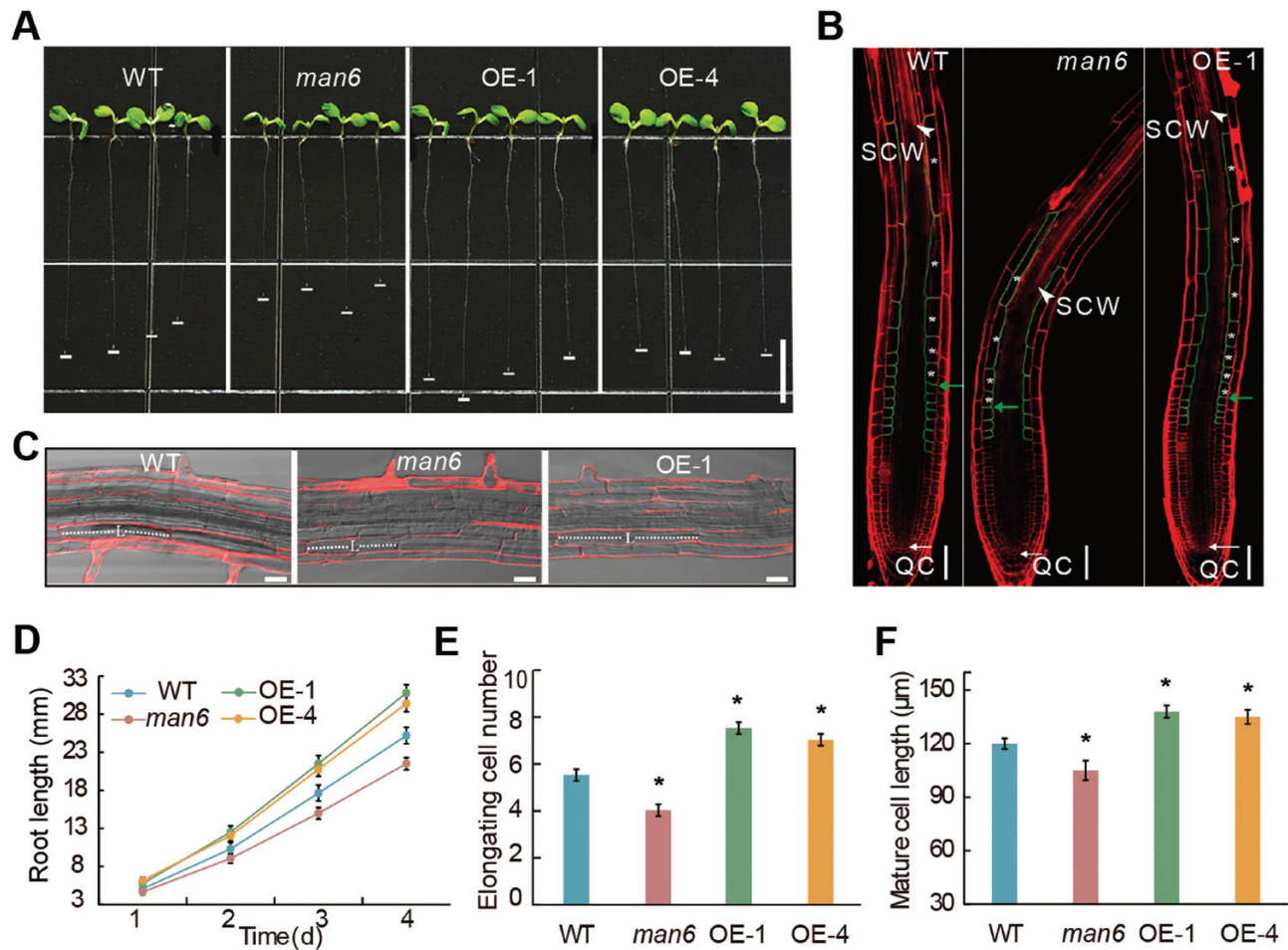


Fig. 2. The influence of *AtMAN6* on root elongation. (A) Root growth of wild-type, *man6*, and *AtMAN6* overexpression seedlings at 7 d. Bar=0.5 cm. (B) Root elongation zones in wild-type, *man6*, and *AtMAN6* overexpression (OE-1) plants staining by PI indicated in red. Asterisks indicate cortical cells that are elongating highlighted by green lines. The occurrence of vessel cells with a SCW is indicated by white arrowheads. The green arrow denotes the starting point for elongation. Bar=30 μm. (C) Root maturation zone in wild-type, *man6*, and *AtMAN6* overexpression (OE-1) plants. The white dotted line represents the length of a mature cortical cell. Bar=30 μm. (D) Root length in wild-type, *man6*, and *AtMAN6* overexpression plants. (E) Number of the cells in the elongation zone. (F) Cortical cell length in the maturation zone. The values in (E) and (F) represent means ±SE, *n*=20. Significance was determined by Fisher's LSD, **P*<0.05.

Table 1. Monosaccharide composition of cell wall hemicelluloses

	WT	<i>man6</i>	OE1	OE4
Xylose	34.87 ± 0.11	45.78 ± 1.19**	28.85 ± 1.95**	23.64 ± 0.44**
Glucose	4.85 ± 0.33	5.08 ± 0.12	5.02 ± 0.17	4.75 ± 0.24
Mannose	5.27 ± 0.17	6.56 ± 0.28**	4.19 ± 0.21*	3.98 ± 0.23**
Galactose	14.21 ± 0.41	14.43 ± 0.42	14.21 ± 0.58	14.60 ± 0.31
Arabinose	9.36 ± 0.61	9.45 ± 0.75	9.67 ± 1.83	9.38 ± 0.03
Fucose	0.75 ± 0.05	0.81 ± 0.06	0.87 ± 0.17	0.81 ± 0.12
Rhamnose	3.62 ± 0.36	3.69 ± 0.56	2.78 ± 0.44	2.60 ± 0.05

Monosaccharide compositions are represented as percentages. The values represent means ±SE, *n*=5. Significance was determined by Fisher's LSD. **P*<0.05; ***P*<0.01.

Meanwhile, *35S:AtMAN6-GFP* transgenic Arabidopsis and their roots were used to investigate the *AtMAN6* subcellular

location. The GFP signal was seen specifically on the plasma membrane (Fig. 4F, G). GFP signal remained on the plasma membrane after treatment with 30% sucrose to induce plasmolysis (Fig. 4H, I).

AtMAN6 has a high hydrolysis activity toward GGM to produce oligosaccharides

To investigate the properties of the *AtMAN6* enzyme, *35S:AtMAN6-7×MYC* transgenic Arabidopsis were generated, and the total proteins were isolated from the rosette leaves of the transgenic and WT plants. Since a low expression level of *AtMAN6* was detected in WT rosette leaves (Supplementary Fig. S3), the following assay results are able to indicate characteristic enzymatic features of *AtMAN6*. To investigate potential *AtMAN6* substrates, glucomannan, galactomannan, mannan,

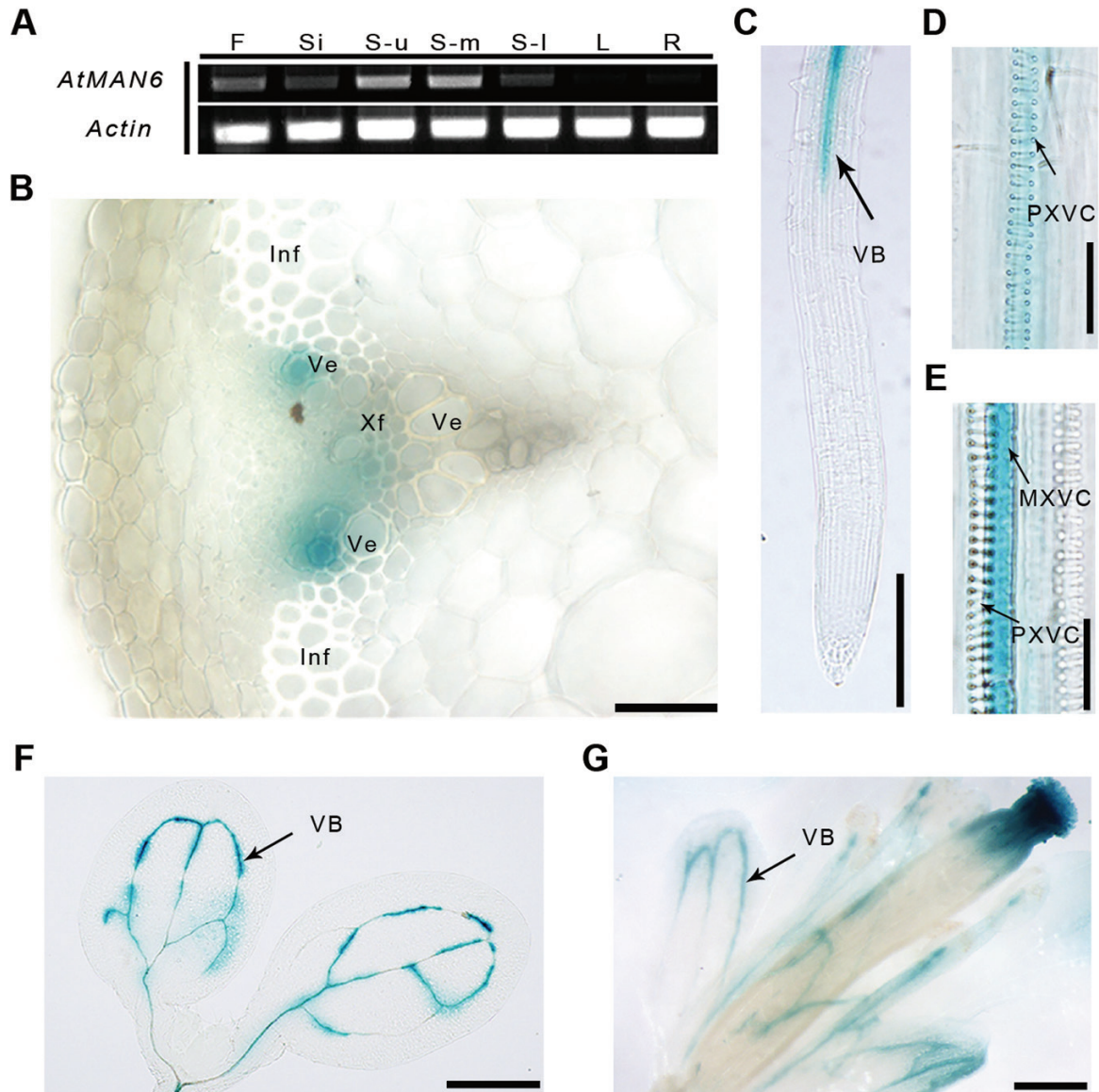


Fig. 3. *AtMAN6* expression profiling and promoter activity. (A) *AtMAN6* expression profiles in various *Arabidopsis* tissues. *AtActin2* was used as an internal reference. The experiment was repeated using three batches of plants. F, flower; Si, silique; S-u, stem of upper part; S-m, stem of middle part; S-l, stem of lower part; L, rosette leaf; R, root. (B–G) GUS staining of the transgenic plants expressing *AtMAN6pro:GUS*. (B) Vascular bundle of inflorescence stem. (C) Root. (D) Root protoxylem vessel cells (PXVC). (E) Root metaxylem vessel cells (MXVC). (F) Cotyledon. (G) Flower. VB, vascular bundle; Ve, vessel cell; Xf, xylem fiber cell; Inf, interfascicular fiber cell. Bar=400 μ m in (F) and (G), 200 μ m in (C), 50 μ m in (B), and 20 μ m in (D) and (E).

xyloglucan, xylan, and carboxymethyl cellulose were purchased, and GGM was extracted from poplar developing xylem tissues and subjected to digestion by *AtMAN6* from rosette leaves of *35S:AtMAN6-7 \times MYC* transgenic *Arabidopsis* under optimal conditions (see the Materials and methods). *AtMAN6* has the highest hydrolysis activity toward GGM and medium activity against other mannan-type polysaccharides such as mannan, glucomannan, and galactomannan. Other non-mannan-type polysaccharides, such as xyloglucan, xylan, and carboxymethyl cellulose, are not hydrolyzed by *AtMAN6* (Fig. 5A). Because *AtMAN6* has the highest hydrolysis activity on GGM, the

production was investigated using HPLC/QTOF-MS and endo-1,4-mannanase (E-BMANN) from *A. niger* as a control. E-BMANN generated oligosaccharides (GGMOs-EMan) with lower molecular weight that include <6 monosaccharide units [degree of polymerization (DP) 6] (Fig. 5B; Supplementary Fig. S4A). The products of *AtMAN6* hydrolysis contained oligosaccharides (GGMOs-Man6) with a higher molecular weight from DP2–DP12, and the products of DP7–DP12 comprised ~2.0% (Fig. 5B; Supplementary Fig. S4B). Furthermore, employing AZCL-galactomannan as a substrate, *AtMAN6* demonstrated the maximum activity at ~pH 5.0 and 45 $^{\circ}$ C (Fig. 5C, D).

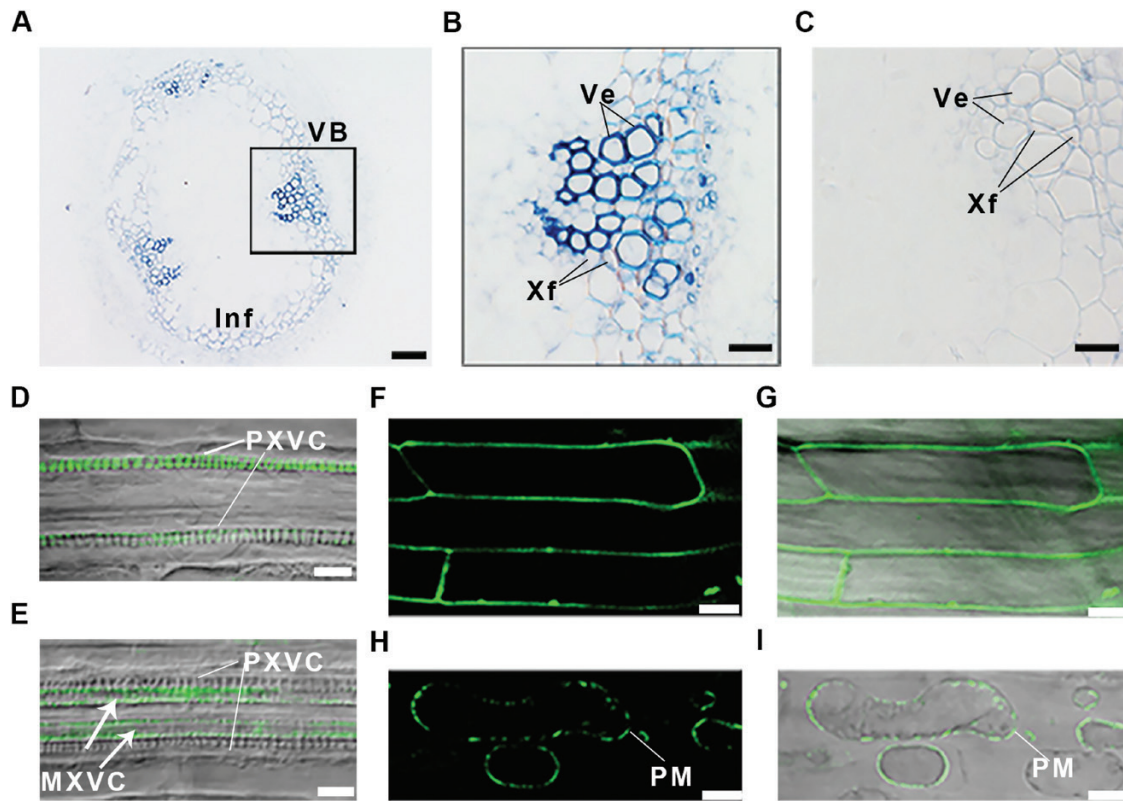


Fig. 4. Localization of AtMAN6. (A and B) Cross-sections of inflorescence stem hybridized with anti-AtMAN6 antibody. (C) Cross-sections of inflorescence stem hybridized with pre-immune IgG as negative control. (D and E) GFP signals in protoxylem vessel cells (D) and metaxylem vessel cells (E) of roots in *AtMAN6pro:AtMAN6-GFP* transgenic plants. (F and G) GFP signals on root epidermal cells of *35S:AtMAN6-GFP* transgenic plant seedlings. (H and I) GFP signals on the plasma membrane by treatment with 30% sucrose on root epidermal cells of *35S:AtMAN6-GFP* transgenic plant seedlings. VB, vascular bundle; Ve, vessel cell; Xf, xylem fiber cell; Inf, interfascicular fiber cell; PXVC, protoxylem vessel cell; MXVC, metaxylem vessel cell; PM, plasma membrane. Bar=50 μm in (A), 20 μm in (B–E), and 10 μm in (F–I).

AtMAN6-type endo-1,4-mannanases in spermatophytes have a characteristic structure

To learn more about the role of MAN6 in plant vascular development, we searched for and examined *MAN6* homologs in a wide variety of plant species including algae, mosses, ferns, gymnosperms, and angiosperms. Using the amino acid sequences of the AtMAN6 protein as a query, we ran BLAST searches in Phytozome version 12.1 and PLAZA (<https://bioinformatics.psb.ugent.be/plaza/>). Based on the conservation of the GH5 glycoside hydrolase domain and the C-terminal cysteine repeat motif 'CSWK/RCKWGCCKK/R', homologous proteins with high sequence similarity to AtMAN6 were identified (Supplementary Table S2). It is worth mentioning that *MAN6* genes are found in spermatophytes, including all of the gymnosperm and angiosperm species investigated, but not in ferns, mosses, or green algae. The significance of the conserved C-terminal cysteine repeat motif was investigated for its subcellular localization. Full-length AtMAN6 protein was located at the plasma membrane (Fig. 6A–C), whereas C-terminal-truncated AtMAN6 protein was detected in both the cytoplasm and the plasma membrane (Fig. 6D–F),

indicating that the C-terminal cysteine repeat motif influences plasma membrane localization. On the other hand, native gel electrophoresis of the AtMAN6 protein isolated from *35S:AtMAN6-7×MYC* plants revealed that AtMAN6 can form a homodimer structure, with the dimer converting to a monomer under reducing conditions (Fig. 6G). Under reducing conditions, AtMAN6 activity was drastically reduced (Fig. 6H). Cysteines were replaced with serine at the 12th N-terminal and 222nd sites of the GH5 domain designated C12S or the conserved C-terminal cysteine repeat motif (423rd, 427th, and 431st) designated C345S to investigate whether the cysteines mediate homodimer formation. Repeated analyses under non-reducing conditions revealed that C12S consistently exhibited both dimer (140 kDa) and monomer (70 kDa) forms, matching WT AtMAN6, whereas C345S only presented one monomer form, a single 70 kDa band (Fig. 6I; Supplementary Fig. S5). The C12S enzymatic activity remained unchanged, whereas the C345S enzymatic activity was significantly reduced (Fig. 6J). This leads to the conclusion that cysteines in the conserved C-terminal cysteine repeat motif of AtMAN6 are necessary for homodimerization and hydrolysis activity.

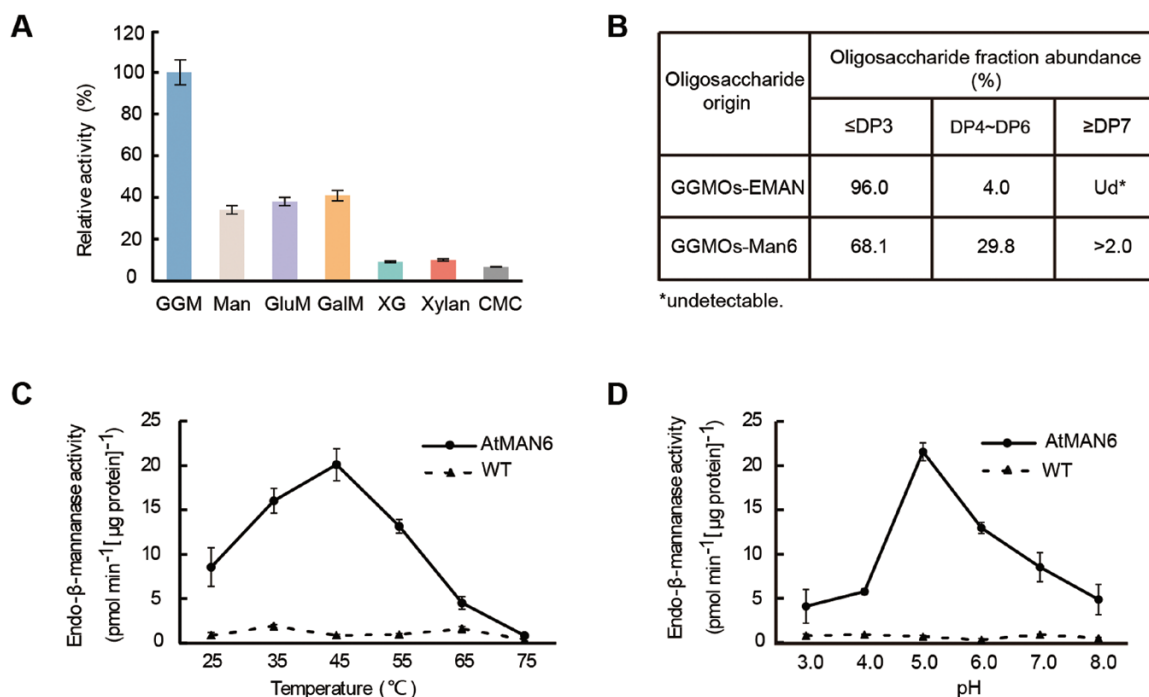


Fig. 5. Characterization of AtMAN6 activity. (A) Substrate specificity of AtMAN6. GGM, glactoglucmannan, Man, mannann, GluM, glucomannan, GalM, galactomannan, XG, xyloglucan, CMC, carboxymethyl cellulose. (B) Relative percentages of identified oligosaccharides in hydrolysis products of AtMAN6 proteins (GGMOs-Man6) and E-BMANN (GGMOs-EMan). (C) Effect of temperature on AtMAN6 enzymatic activity. (D) Effect of pH on AtMAN6 enzymatic activity. AtMAN6, total proteins from the rosette leaves of 35S:AtMAN6 transgenic plants; WT, total proteins from the rosette leaves of the wild type.

GGMOs impede secondary cell wall deposition in both vessel cells and their neighboring fiber cells

Although AtMAN6 is only expressed in vessel cells of vascular tissues, the *man6* mutant and OE plants showed an influence on fiber cell elongation growth in both the root and inflorescence stem. We proposed that the products of AtMAN6 serve as a signal for the regulation of SCW deposition in vascular tissues. To test the hypothesis, the products of AtMAN6 (GGMOs-Man6) and E-BMANN (GGMOs-EMan) were utilized to treat WT seedlings (Fig. 7A–D) and inflorescence stems (Fig. 7E–H). When GGMOs-Man6 seedlings were compared with GGMOs-EMan and the negative control, root length and cell number in the elongation zone before vessel cell appearance were significantly increased (Fig. 7A–D), and treatment with GGMOs resulted in no morphological change in the root apical meristem (Supplementary Fig. S6). Inflorescence stems that had not yet produced SCWs in the interfascicular cells (Fig. 7E) were supplied GGMOs-Man6, GGMOs-EMan, and the control buffer. The negative control and GGMOs-EMan both caused the interfascicular fiber cells to deposit obvious SCWs (Fig. 7F, G), while GGMOs-Man6 did not (Fig. 7H). According to the findings, AtMAN6 products can suppress SCW formation during inflorescence stem development.

The transcription of genes involved in secondary cell wall biosynthesis was regulated by AtMAN6

To examine the molecular mechanisms underpinning AtMAN6 regulation, RNA-seq was employed to assess transcriptional profiles in the inflorescence stems of *man6* mutant, OE, and WT plants. The analysis of the differentially expressed genes (DEGs) revealed that in the *man6* mutant, 312 genes (~1% of the total identified genes) were up-regulated whereas 306 genes were down-regulated (Supplementary Fig. S7A; Supplementary Table S3). In the OE plants, 355 genes (~1% of all observed genes) were up-regulated, while 524 genes (~2% of all detected genes) were down-regulated (Supplementary Fig. S7C; Supplementary Table S4). Based on the Gene Ontology (GO) annotation, these DEGs were categorized into five categories: cell wall biosynthesis, signal transduction, cellular process, metabolism, and others. Among these categories, cell wall biosynthesis and signal transduction were over-represented in both *man6* mutant and OE plants (Supplementary Fig. S7B, D). Several SCW-related genes, including the key TF genes *SND1*, *NST1*, *VND6*, and *MYB46*, as well as the cellulose and lignin biosynthesis genes *CESA4*, *CESA7*, *PAL*, and *4CL1*, were considerably up-regulated in the mutant but down-regulated in the OE plants (Fig. 8A). Furthermore, the expression of TFs involved in the ethylene and jasmonic acid signaling pathways changed significantly in the mutant and OE plants. *ERF109*,

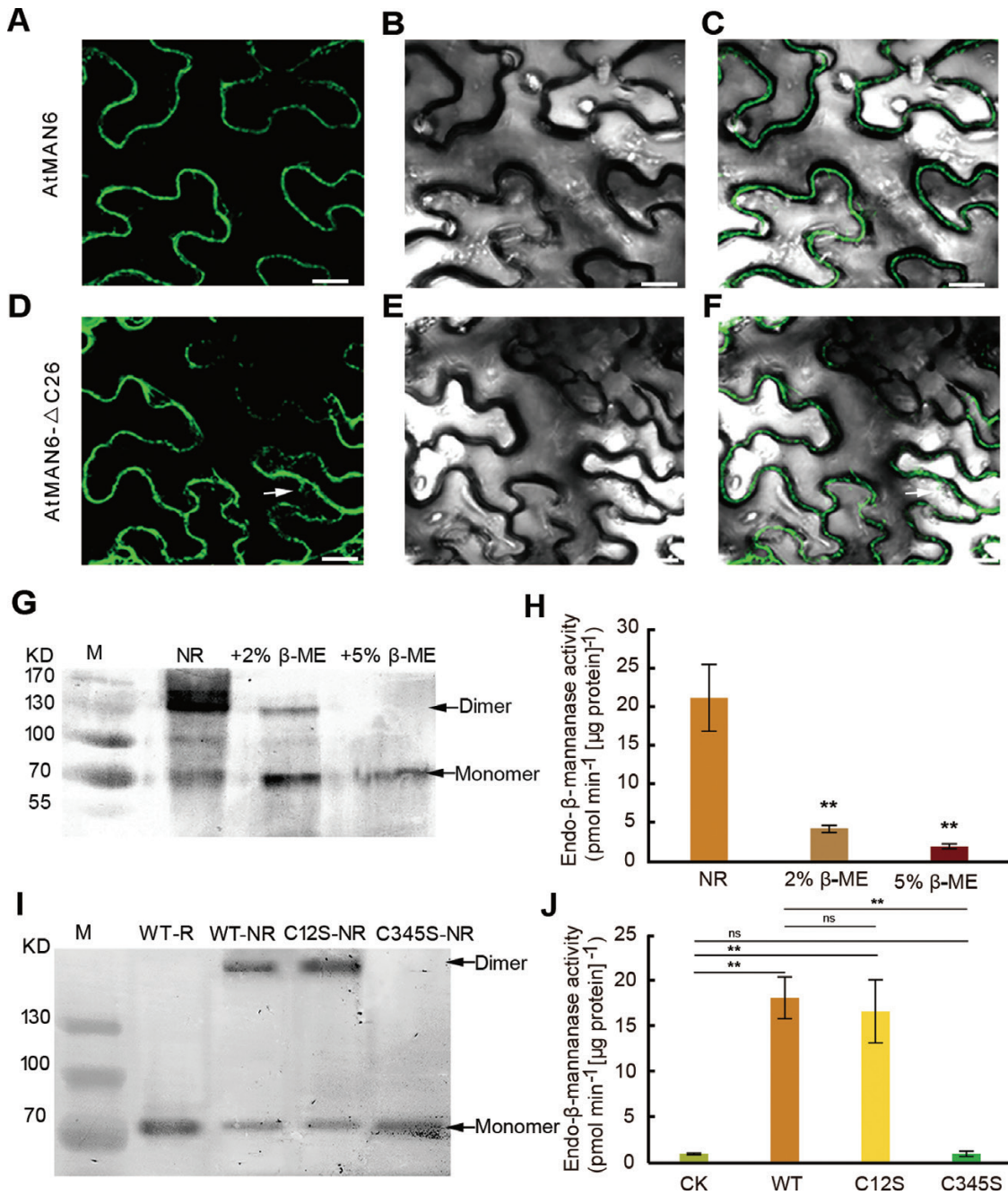


Fig. 6. The conserved C-terminal cysteine repeat motif-mediated dimerization of MAN6 is essential for both subcellular location and enzymatic activity. (A–C) Transient expression of *35S:AtMAN6-GFP* in tobacco leaf epidermal cells. Bar=20 μm. (D–F) Transient expression of *35S:AtMAN6ΔC26-GFP* in tobacco leaf epidermal cells; bar=20 μm. (G) Dimer formation of native AtMAN6 protein. M, molecular mass standard. NR, AtMAN6 protein under non-reducing conditions. +2% β-ME and +5% β-ME, AtMAN6 protein under reducing conditions with 2% or 5% β-mercaptoethanol, respectively. Arrows indicate the monomer and dimer of AtMAN6. (H) Effect of dimerization on AtMAN6 enzymatic activity. The values represent means ±SE, *n*=3. (I) The C-terminal cysteine repeat motif mediates dimerization. AtMAN6-R, AtMAN6–GFP fusion protein under reducing (R) conditions; AtMAN6-NR, AtMAN6–GFP fusion protein under non-reducing (NR) conditions. C12S-NR, AtMAN6(C12S)–GFP fusion protein under non-reducing conditions. C345S-NR, AtMAN6 (C345S)–GFP fusion protein under non-reducing conditions. GFP antibodies were used to detect the bands. (J) Effect of cysteine mutations of the C-terminal cysteine repeat motif on AtMAN6 enzymatic activity. CK means proteins from *35S:GFP* transgenic plants. The values represent means ±SE, *n*=3. Significance was determined by Fisher's LSD, **P*<0.05, ***P*<0.01.

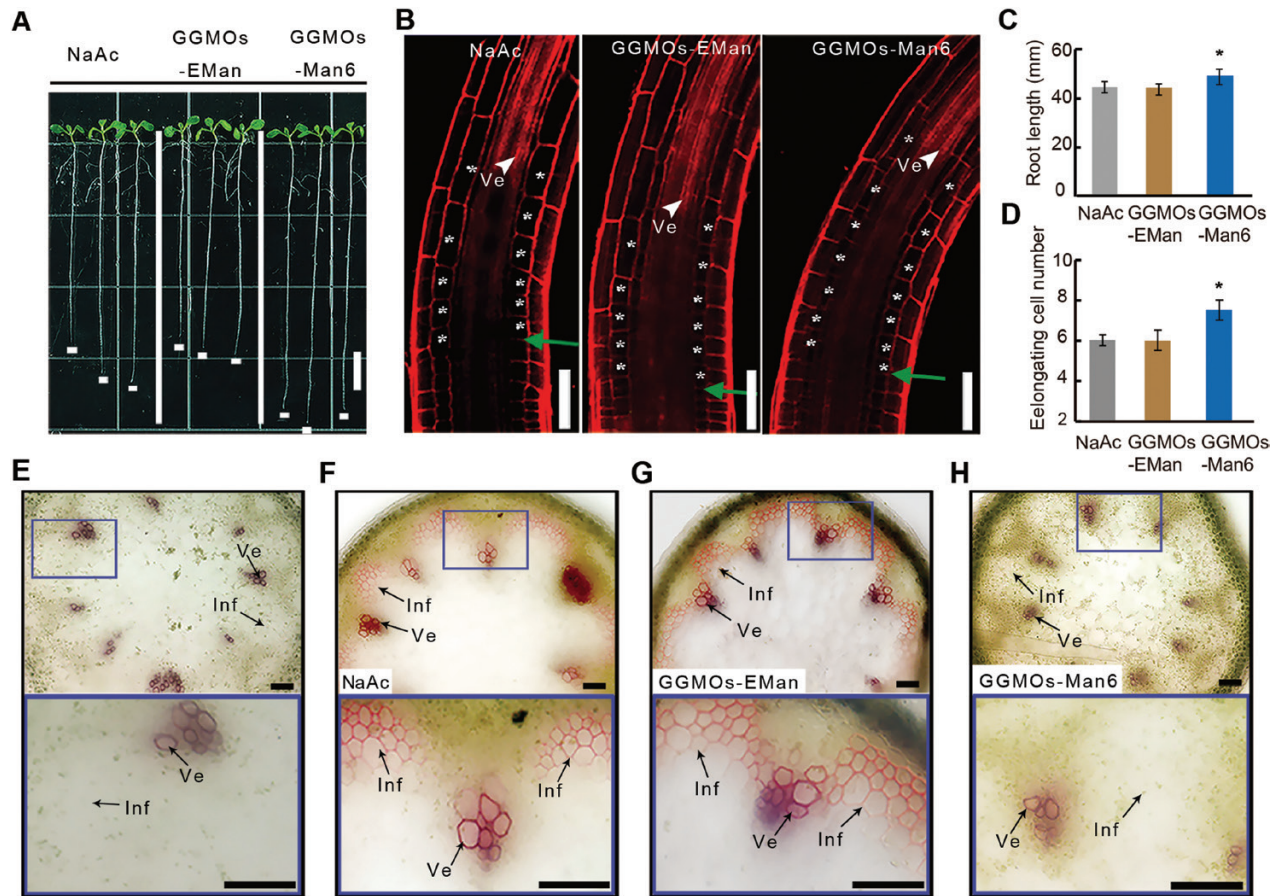


Fig. 7. Effect of GGMO treatment on root elongation and interfacicular fiber SCW deposition. (A) Wild-type seedlings after GGMO treatment. Bar=1 cm. (B) Root elongation zone stained by PI after NaAc buffer, GGMOs-Eman, and GGMOs-Man6 treatment. Asterisks mark elongating cortex cells. White arrowheads mark the occurrence of vessel cells. Bar=50 μ m. (C) Quantification of root length after GGMO treatment. (D) Quantification of elongating cortex cell number after GGMO treatment. The values represented in (C) and (D) are means \pm SE, $n=20$. Significance was determined by Fisher's LSD, $*P<0.05$. (E) Cross-sections of inflorescence stems before GGMO treatment. (F) Cross-sections of inflorescence stems after NaAc buffer treatment as control. (G) Cross-sections of inflorescence stems after GGMOs-EMan treatment. (H) Cross-sections of inflorescence stems after GGMOs-Man6 treatment. Arrows indicate interfacicular fiber cells and vessel cells stained with 0.5% (w/v) phloroglucinol in 12% HCl and bar=50 μ m in (E–H).

ERF1, and *ORA59*, for example, which were positive regulators of the two signaling pathways, were up-regulated in the mutant and down-regulated in the OE plants, whereas *WRKY54*, a negative regulator of the jasmonic acid signaling pathway, was down-regulated in the mutant and up-regulated in the OE plants (Supplementary Fig. S7E). RT-qPCR analysis validated the expression changes in these genes in *man6* mutant and OE plants (Fig. 8A; Supplementary Fig. S7E). These findings suggested that *AtMAN6*–GGMO signaling can impact the transcriptional network of SCW biosynthesis during xylem cell development (Fig. 8B).

Discussion

Cell expansion and SCW deposition in vascular tissues control cell size and mechanical characteristics. However, it is unknown how cells sense their final size in order to proceed with the subsequent developmental phase and SCW deposition. We

provided genetic, biochemical, and morphological evidence in this study to show that *AtMAN6*, an endo-1,4-mannanase, promotes vessel cell expansion by hydrolyzing GGMs in its cell walls, and that its catalytic product, GGMOs, as a signal, inhibit SCW deposition in both vessel cells and their neighbor fiber cells during xylem differentiation.

We demonstrated that both the *AtMAN6* transcript and its encoded protein can be detected only during the early stages of vessel cell development. *AtMAN6* expression patterns indicate that its developmental role is specifically limited to the early period of vessel cell growth. We also discovered that overexpression of *AtMAN6* results in longer roots and delayed deposition of SCWs in root vascular tissues, as well as smaller size of vascular cells with thinner SCWs in the stem. The rationale could be that *AtMAN6* promotes cell expansion by changing the PCW properties while suppressing SCW deposition. Unlike other types of MANs that are found in cell walls (Bewley *et al.*, 2000; Rodríguez-Gacio *et al.*, 2012), *AtMAN6* is

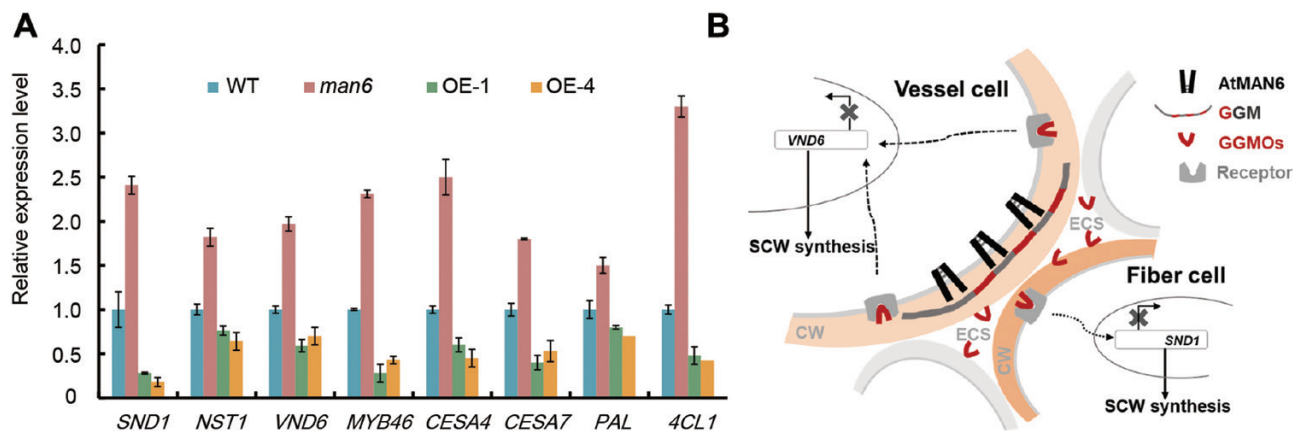


Fig. 8. The impact of *AtMAN6* on the expression of genes involved in SCW biosynthesis and a proposed working model. (A) Relative expression levels of SCW biosynthesis-associated genes in wild-type, *man6* mutant, and *AtMAN6* overexpression lines. The *AtActin2* gene was used as an internal reference. The values represent means \pm SE, $n=3$. (B) The working model of *AtMAN6* and its production of GGMOs during expansion of the vessel cell and deposition of SCW in both the vessel cell and its neighbor fiber cell. *AtMAN6* was expressed in the plasma membrane of the vessel cell at the early development stage and hydrolyzed GGMs in the primary cell walls into GGMOs, which could be recognized by certain receptor(s) on the plasma membrane of both vessel cells and neighbor fiber cells. The *AtMAN6*–GGMO signaling further repressed expression of the transcriptional switch of SCW biosynthesis, which allows expansion of vessel cell spatiotemporally.

specifically located in the plasma membrane of vessel cells. The GFP signals appear in the plasma membrane of the root epidermal cells of *35S:AtMAN6-GFP* transgenic seedlings (Fig. 4E, G). To confirm the plasma membrane localization, 30% sucrose was employed to cause plasmolysis of the seedlings; the GFP signals remained on the plasma membrane (Fig. 4H, I). Additionally, sequence alignments of *AtMAN6* and *PtrMAN6* show a similarity of the N-terminal signal peptide, which has been proven to be in charge of the proteins' plasma membrane localization and the presence of their active domain outside the plasma membrane in previous studies (Zhao *et al.*, 2013a, b). It is noteworthy that *AtMAN6* does not possess a transmembrane domain, yet it is shown to be localized on the transmembrane. There is a potential association between *AtMAN6* and the plasma membrane, which may occur through its interaction with other proteins. However, further study is necessary in order to thoroughly investigate this issue.

Because of its plasma membrane location, *AtMAN6* appears to have a restricted impact, possibly influencing only cell wall modification in vessel cells. Our data revealed that the *man6* mutant and *AtMAN6* overexpression impacted vessel cells locally as well as neighboring fiber cells in vascular tissues. One possibility is that vessel cells generate a signal that regulates SCW formation in both fiber and vessel cells. *AtMAN6* has a unique ability to hydrolyze GGM to produce GGMOs. The administration of GGMOs in both the root and stem delays the formation of SCWs in vascular cells. The data imply that GGMOs can influence SCW deposition in vascular cells. Due to its positioning at the plasma membrane, *AtMAN6* exhibits its active domain externally, enabling its involvement in the hydrolysis process of cell wall GGM. This enzymatic activity results in the production of GGMOs within the apoplast. The perception mechanism of GGMO signaling remains unclear,

although it is conceivable that nearby cells may possess a receptor located in the plasma membrane, enabling them to readily detect the GGMO signal present in the apoplast (Seifert and Blaukopf, 2010) (Fig. 8B).

AtMAN6 is pH sensitive, having its highest enzymatic activity at pH 5.0, which is comparable with the pH in the extracellular environment (Barbez *et al.*, 2017). GGMOs derived from *MAN6* hydrolysis demonstrated biological activity in inhibiting SCW synthesis during cell growth and differentiation in both vessel and fiber cells. SCW deposition must be inhibited when cells are expanding in order to facilitate cell enlargement. *MAN6* may detect the extracellular environment, which controls *MAN6* hydrolysis activity to govern cell expansion, and GGMOs produced by *MAN6* hydrolysis may operate as an inhibitor to control the initiation of SCW synthesis. Cell wall oligosaccharides have been demonstrated to behave as signals impacting developmental processes (Mohnen and Hahn, 1993). Typically, oligosaccharide biological activity is determined by their degree of polymerization, methylation, and conformation (Seifert and Blaukopf, 2010). In our study, the DP7–DP12 oligomers generated by *MAN6* hydrolysis were found to be distinct from the oligosaccharides of other *MAN* digestion products. This portion of oligomers may be responsible for the detected GGMO activity. Although more studies are required to determine the specific structure of the active oligomer, the genetic involvement of *AtMAN6* in increasing vascular cell elongation as well as regulating SCW synthesis is supported by the *AtMAN6*-derived oligosaccharide activity. This study added to our understanding of the coordinative regulation of cell elongation and SCW deposition during vascular development.

The examination of transcriptional profiling in the *man6* mutant and the OE transgenic plants provided a preliminary idea of the downstream signaling of GGMOs. A significant

proportion of the genes exhibiting differential expression are associated with the synthesis of the cell wall, as indicated in [Supplementary Tables S3](#) and [S4](#). The expression levels of genes that synthesize cellulose and lignin were mostly higher in the *man6* mutant and lower in the OE plants. These genes include *CESA4*, *CESA7*, and *CESA8*, which are involved in SCW cellulose synthesis, and *PAL* and *4CL1*, which synthesize monolignols in SCW. These findings suggest that there is a modification in the biosynthesis of the SCW in these plants. In the same way, it was found that TF genes such as *SND1*, *NST1*, *VND6*, and *MYB46*, which control the biosynthesis of the SCW, were up-regulated in the *man6* mutant and down-regulated in the OE plants. This indicates that MAN6 plays a crucial role in mediating the signaling pathways involved in the regulation of SCW formation. Further investigation is required to understand how GMOs, derived due to the function of MAN6, act as a signal in regulating the deposition of SCW in the vascular tissue cells, including both the vessel and surrounding fiber cells. A crucial step in this research would be to identify the putative receptor responsible for perceiving the GMO signal.

Supplementary data

The following supplementary data are available at [JXB online](#).

Fig. S1. Analysis of the T-DNA insertion *man6* mutant and *35S:AtMAN6* overexpression in *Arabidopsis*.

Fig. S2. Validation of AtMAN6 antibody specificity.

Fig. S3. Expression profile of *AtMAN* genes in various tissues.

Fig. S4. AtMAN6 enzymic activity analysis.

Fig. S5. A repeat result in support of that shown in [Fig. 6I](#).

Fig. S6. Effect of GGMO treatment on root.

Fig. S7. Transcriptome analysis of *man6* mutant and overexpression plants.

Table S1. Primers used in this study.

Table S2. List of the plant species examined for *AtMAN6* homologs in this work.

Table S3. List of the DEGs in the *man6* mutant.

Table S4. List of the DEGs in *AtMAN6* overexpression plants.

Acknowledgements

We thank Mr Wenli Hu for assistance with the GC-MS and HPLC/QTOF-MS analysis (CEPAMS), and Mr Xiaoyan Gao for assistance with TEM assay (CEPAMS).

Author contributions

LL: conceptualization; RZ and BL: performing the experiments; YJZ: providing suggestions and data analysis; YYZ and LL: data analysis and writing. All authors have read and approved the final manuscript.

Conflict of interest

No conflict of interest declared.

Funding

This work was supported by the National Nature Science Foundation of China (32130072 to LL and 31901329 and 32271827 to YZ), and the Strategic Priority Research Program of the Chinese Academy of Sciences (XDB27020104 to LL).

Data availability

The RNA-seq data underlying this article are available in the Gene Expression Omnibus (GEO) database at (<https://www.ncbi.nlm.nih.gov/geo/>) and can be accessed with accession number GSE243854.

References

- Barbez E, Dünser K, Gaidora A, Lendl T, Busch W.** 2017. Auxin steers root cell expansion via apoplastic pH regulation in *Arabidopsis thaliana*. *Proceedings of the National Academy of Sciences, USA* **114**, E4884–E4893.
- Barnes WJ, Anderson CT.** 2018. Release, recycle, rebuild: cell-wall remodeling, autodegradation, and sugar salvage for new wall biosynthesis during plant development. *Molecular Plant* **11**, 31–46.
- Benová-Kákosová A, Digonnet C, Goubet F, et al.** 2006. Galactoglucomannans increase cell population density and alter the protoxylem/metaxylem tracheary element ratio in xylogenic cultures of *Zinnia*. *Plant Physiology* **142**, 696–709.
- Bewley JD, Banik M, Bourgault R, Feurtado JA, Toorop P, Hilhorst HW.** 2000. Endo-beta-mannanase activity increases in the skin and outer pericarp of tomato fruits during ripening. *Journal of Experimental Botany* **51**, 529–538.
- Clough SJ, Bent AF.** 1998. Floral dip: a simplified method for *Agrobacterium*-mediated transformation of *Arabidopsis thaliana*. *The Plant Journal* **16**, 735–743.
- Cosgrove DJ.** 2016. Catalysts of plant cell wall loosening. *F1000Research* **5**, F1000 Faculty Rev-119.
- Cosgrove DJ.** 2022. Building an extensible cell wall. *Plant Physiology* **189**, 1246–1277.
- Foster CE, Martin TM, Pauly M.** 2010a. Comprehensive compositional analysis of plant cell walls (lignocellulosic biomass) part I: lignin. *Journal of Visualized Experiments* **37**, 1745.
- Foster CE, Martin TM, Pauly M.** 2010b. Comprehensive compositional analysis of plant cell walls (lignocellulosic biomass) part II: carbohydrates. *Journal of Visualized Experiments* **37**, 1837.
- Kollárová K, Vatehová Z, Slováková L, Lišková D.** 2010. Interaction of galactoglucomannan oligosaccharides with auxin in mung bean primary root. *Plant Physiology and Biochemistry* **48**, 401–406.
- Kubo M, Udagawa M, Nishikubo N, Horiguchi G, Yamaguchi M, Ito J, Mimura T, Fukuda H, Demura T.** 2005. Transcription switches for protoxylem and metaxylem vessel formation. *Genes & Development* **19**, 1855–1860.
- Luo L, Zhu Y, Gui J, Yin T, Luo W, Liu J, Li L.** 2021. A comparative analysis of transcription networks active in juvenile and mature wood in *Populus*. *Frontiers in Plant Science* **12**, 675075.
- McCarthy RL, Zhong R, Ye Z-H.** 2009. MYB83 is a direct target of SND1 and acts redundantly with MYB46 in the regulation of secondary cell wall biosynthesis in *Arabidopsis*. *Plant and Cell Physiology* **50**, 1950–1964.

- Meents MJ, Watanabe Y, Samuels AL.** 2018. The cell biology of secondary cell wall biosynthesis. *Annals of Botany* **121**, 1107–1125.
- Mitsuda N, Seki M, Shinozaki K, Ohme-Takagi M.** 2005. The NAC transcription factors NST1 and NST2 of *Arabidopsis* regulate secondary wall thickenings and are required for anther dehiscence. *The Plant Cell* **17**, 2993–3006.
- Mohnen D, Hahn MG.** 1993. Cell wall carbohydrates as signals in plants. *Seminars in Cell Biology* **4**, 93–102.
- Moreira LRS, Filho EXF.** 2008. An overview of mannan structure and mannan-degrading enzyme systems. *Applied Microbiology and Biotechnology* **79**, 165–178.
- Park YB, Cosgrove DJ.** 2012. A revised architecture of primary cell walls based on biomechanical changes induced by substrate-specific endoglucanases. *Plant Physiology* **158**, 1933–1943.
- Puls J.** 1997. Chemistry and biochemistry of hemicelluloses: relationship between hemicellulose structure and enzymes required for hydrolysis. *Macromolecular Symposia* **120**, 183–196.
- Rao X, Dixon RA.** 2018. Current models for transcriptional regulation of secondary cell wall biosynthesis in grasses. *Frontiers in Plant Science* **9**, 399.
- Rodríguez-Gacio MC, Iglesias-Fernández R, Carbonero P, Matilla AJ.** 2012. Softening-up mannan-rich cell walls. *Journal of Experimental Botany* **63**, 3976–3988.
- Scheller HV, Ulvskov P.** 2010. Hemicelluloses. *Annual Review of Plant Biology* **61**, 263–289.
- Seifert GJ, Blaukopf C.** 2010. Irritable walls: the plant extracellular matrix and signaling. *Plant Physiology* **153**, 467–478.
- Song D, Shen J, Li L.** 2010. Characterization of cellulose synthase complexes in *Populus* xylem differentiation. *New Phytologist* **187**, 777–790.
- Sparkes IA, Runions J, Kearns A, Hawes C.** 2006. Rapid, transient expression of fluorescent fusion proteins in tobacco plants and generation of stably transformed plants. *Nature Protocols* **1**, 2019–2025.
- Tang W, Coughlan S, Crane E, Beatty M, Duvick J.** 2006. The application of laser microdissection to *in planta* gene expression profiling of the maize anthracnose stalk rot fungus *Colletotrichum graminicola*. *Molecular Plant-Microbe Interactions* **19**, 1240–1250.
- Whitney SEC, Brigham JE, Darke AH, Reid JSG, Gidley MJ.** 1998. Structural aspects of the interaction of mannan-based polysaccharides with bacterial cellulose. *Carbohydrate Research* **307**, 299–309.
- Wolf S.** 2022. Cell wall signaling in plant development and defense. *Annual Review of Plant Biology* **73**, 323–353.
- Yamaguchi M, Kubo M, Fukuda H, Demura T.** 2008. VASCULAR-RELATED NAC-DOMAIN7 is involved in the differentiation of all types of xylem vessels in *Arabidopsis* roots and shoots. *The Plant Journal* **55**, 652–664.
- Yu L, Chen H, Sun J, Li L.** 2014. *PtrKOR1* is required for secondary cell wall cellulose biosynthesis in *Populus*. *Tree Physiology* **34**, 1289–1300.
- Yu L, Lyczakowski JJ, Pereira CS, Kotake T, Yu X, Li A, Mogelsvang S, Skaf MS, Dupree P.** 2018. The patterned structure of galactoglucomannan suggests it may bind to cellulose in seed mucilage. *Plant Physiology* **178**, 1011–1026.
- Yu L, Sun J, Li L.** 2013. *PtrCel9A6*, an endo-1,4- β -glucanase, is required for cell wall formation during xylem differentiation in *Populus*. *Molecular Plant* **6**, 1904–1917.
- Yu L, Yoshimi Y, Cresswell R, et al.** 2022. Eudicot primary cell wall glucomannan is related in synthesis, structure, and function to xyloglucan. *The Plant Cell* **34**, 4600–4622.
- Zhao Y, Song D, Sun J, Li L.** 2013a. *Populus* endo-beta-mannanase PtrMAN6 plays a role in coordinating cell wall remodeling with suppression of secondary wall thickening through generation of oligosaccharide signals. *The Plant Journal* **74**, 473–485.
- Zhao Y, Zhang Q, Yuan L, Zhang R, Li L.** 2013b. N-glycosylation and dimerization regulate the PtrMAN6 enzyme activity that may modulate generation of oligosaccharide signals. *Plant Signaling & Behavior* **8**, e26956.
- Zhong R, Cui D, Ye Z-H.** 2019. Secondary cell wall biosynthesis. *New Phytologist* **221**, 1703–1723.
- Zhong R, Demura T, Ye Z-H.** 2006. SND1, a NAC domain transcription factor, is a key regulator of secondary wall synthesis in fibers of *Arabidopsis*. *The Plant Cell* **18**, 3158–3170.
- Zhong R, Richardson EA, Ye Z-H.** 2007. Two NAC domain transcription factors, SND1 and NST1, function redundantly in regulation of secondary wall synthesis in fibers of *Arabidopsis*. *Planta* **225**, 1603–1611.
- Zhu Y, Li L.** 2021. Multi-layered regulation of plant cell wall thickening. *Plant & Cell Physiology* **62**, 1867–1873.